Experimental and Numerical Study of Flow and Heat Transfer due to Intermittent Impinging Mist Jets

A. D. Nazarov*, M. A. Pakhomov, A. F. Serov, V. I. Terekhov
Kutateladze Institute of Thermophysics, Siberian Branch of Russian Academy of Sciences, 1, Acad. Lavrent'ev Avenue, Novosibirsk, Russia.
nazarov@itp.nsc.ru, pakhomov@ngs.ru, serov@itp.nsc.ru, terekhov@itp.nsc.ru

Abstract

The flow structure and heat transfer of an intermittent impinging mist jet is studied experimentally and numerically (with low mass concentration of droplets not more than 1 %). In the range of distances between the tube edge and target $H/(2R) \leq 6$ heat transfer at stagnation point increases with a rise of pulsation frequency, whereas at high distances $H/(2R) > 8$ frequency rise causes heat transfer reduction. Heat transfer intensity during flow pulse action increases and exceeds significantly the corresponding value for the steady-state case. At time moment, when there is no flow, the value of Nusselt number decreases considerably. Results obtained are compared with available data of other authors, and satisfactory agreement is obtained for the influence of pulsation frequency on heat transfer of the gas jet with impinging surface.

Introduction

Impinging gas or mist jet is employed in many industrial applications (for example drying of sheets of various materials, cooling of electronic devices and gas turbines blades, printing and painting processes, etc) due to significant heat and mass transfer enhancement around the stagnation point [1],[2],[3],[4]. In many technical applications intermittent (pulsed) flow occurs due to moving parts, by vibrations or flow oscillations. Studies performed show a complex physical situation that in some cases leads to significant heat transfer enhancement, however, a decrease in heat transfer can also occur [5],[6],[7],[8],[9]. Spray impingement on hot surfaces has capability of removing large amounts of heat due to the use of latent heat of vaporization. An increase in heat transfer can change from 10 to 100% in vicinity of stagnation point and to 40-50% in the zone of wall jet development. A decrease in heat transfer varies within 10-30% over the whole impinging surface.

An addition of evaporating droplets causes a significant increase in heat transfer intensity in comparison with the single-phase [10],[11],[12],[13],[14]. The impingement of pulsed mist flow on hot surfaces occurs also in practical situations, which require comprehensive knowledge of the flow patterns and interaction of spray with the impinging surface.

The aim of the present work is experimental and numerical simulation of the effect of droplets evaporation on the flow and heat transfer in turbulent impinging pulsed jets.

Setup and Measurement Methods

The experimental setup [13] (Figure 1) consists of the heat exchanger with calorimeter and programmable controllable multinozzle source of pulse spray with separate supply of liquid and gas phases. The main studies have been carried out, when the distance between the heat exchanger and source was L = 230 mm. At this position on a cross-section of heat exchanger surface the source of pulse gas-droplet flow forms a two-phase flow with the area of 300 × 300 mm^2.

The heat exchanger is made of high heat conducting copper with the plane sizes of 140 × 140 mm and thickness of 30 mm. In these experiments we have maintained the constant temperature of heat exchanger surface T_w = const =70 ^{0}C.

The calorimeter is made by the principle of registration of the amount of heat obtained by the heat exchanger from the heat energy source (maximal supplied power of the electric boiler is P = 6 kW) under the dynamic conditions. According to the practice, the total measurement error for the heat flux from the heat exchanger with consideration of heat losses (heat-conducting accessories, etc.) is within 1.5 ÷ 3 %, what allows determination of heat transfer parameters and their dependence on the cooling flow with the permissible error (< 10%). To register fast (< 0.01 s) heat transfer processes, the sensor of local heat flux was mounted in the center of the heat exchanger surface [15].

* Corresponding author: nazarov@itp.nsc.ru

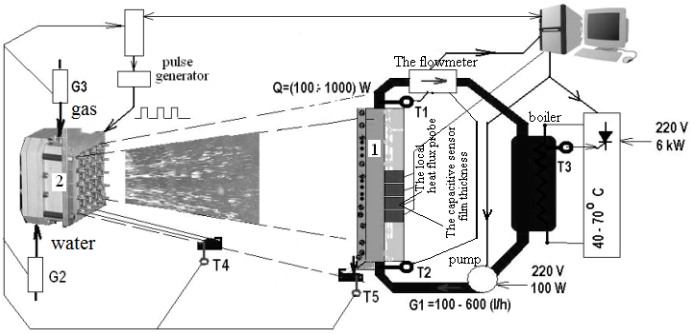

Figure 1 Spray experimental setup.

Output source has sixteen spray liquid in the form of a matrix of 4 × 4 and 25 nozzles with the outlet diameter of 0.35 mm for the co-current air flow.

Liquid dispenser has a solenoid valve. Valve is leaking through the four output ports. Each outlet nozzle has a diameter of 0.125 mm (d). Time of transition from the open valve to the closed (and back) of less than 0.1 ms (t_{tr}). Time t_{on} was varied in the range from 1 to 10 ms. Frequency of valve opening f_i changed from 1 to 50 Hz. Together with parameter t_{on} the pressure at the unit inlet (P_l = 0.05 ÷ 0.6 MPa) effected the liquid flow through the sprayers and droplet size. A change in the pressure allowed formation of the flow with a given velocity of the liquid phase in the range from 0 to 20 ms^{-1}. Each sprayer was calibrated, and the total flow rate of the droplet phase was determined by data obtained.

According to measurements performed at distance L = 0.2 m from the source along the spray cross-section at different pressures at liquid valve and gas nozzle inlets, deviation of the flow density from the average value does not exceed 5% [8]. According to analysis of video records near the plate surface (L ~ 200 mm) we can observe two main sizes of droplets: large (0.12 ÷ 0.15) mm and small ones (0.045 ÷ 0.050) mm.

Pulsed droplet flow moves in a cocurrent air stream, which has a constant speed. Depending on the mode, the air velocity can vary over a wide range (0 ÷ 25 ms^{-1}) by changing the pressure at the inlet. (P_g = 0.05 ÷ 0.6 MPa). The measurements of the air flow velocity have shown that distribution of velocity in the cross-section is uniform distribution over the whole heat exchanging surface.

The interaction of a single aerosol nozzle and the surface is well studied. However, in practice, are increasingly used multinozzle cooling sources, generating a droplet stream inside cocurrent constant air flow. The design of the source of our stand is experimental. And take into account the trend of industrial sources. The aim is to explore the possibilities of development of systems with controlled heat transfer. Depending on the heat load of the heat exchanger, such systems allow you to set parameters of the cooling gas-droplet flow, changing the duration, frequency and place of supply of the liquid component of the flow on the surface of a exchanger, creating the optimum heat transfer.

The experimental results

Heat and mass transfer is measured under the atmospheric conditions and ambient temperature t_0 = 20 ^{0}C. The temperatures of air and liquid aerosol phases are as follows: liquid temperature was (7 ÷ 13)^{0}C; air temperature was (20 ÷ 22)^{0}C; and temperature of the heat exchanger surface was T_w = 70 ^{0}C. The averaged heat transfer coefficient for the heat exchanger surface is determined as $\alpha = Q\ (f\ (T_W - T_l))^{-1}$, where Q is heat energy supplied to the heat exchanger; f is its area, and T_w and T_l are temperatures of the heat exchanging surface and liquid in the spray flow.

Figure 2 demonstrates the effect of frequency and duration of spray supply pulse on the heat transfer coefficient at the constant velocity of the co-current air flow (8 ms^{-1}) and ratio of mean-mass velocities of liquid and gas phases in the range of $\rho_l V_l (\rho_g V_g)^{-1}$ = 0 ÷ 0.01 [14].

At a frequency of 1 Hz for the duration of the opening of the liquid valve 2 ms, the value of the heat transfer coefficient is almost 1.5 times less than the heat transfer coefficient for the duration of the opening of 10 ms (the curves for other situations are in-between them). In both cases on the heat exchanging surface there are the conditions of evaporation cooling, when the liquid part of spray evaporates on the heat exchanging surface before the next portion of spray arrives. A rise of frequency of liquid phase pulses leads to the value of heat transfer coefficient approaches maximum. When the valve is opened during 10 ms, the conditions of evaporation cooling on the heat exchanger surface turn into the conditions of film cooling. For valve opening of 2 ms, cooling stays in the form of evaporation. Under these conditions we can achieve the optimum of cooling efficiency, when the amount of droplets precipitated on the surface is sufficient to complete evaporation by the moment of next portion arrival.

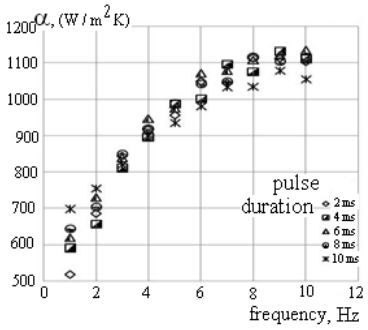

Figure 2 Heat transfer coefficient vs. frequency and duration of spray.

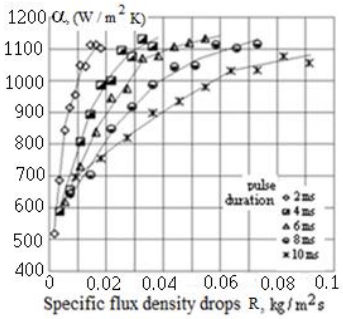

Figure 3 The effect of irrigation rate and pulse duration on the heat transfer coefficient.

The variation of heat transfer coefficient α on liquid mass flow rate R is shown in Figure 3 for different opening conditions of aerosol pulses: t_{on} = 2 ms ÷ 10 ms, f_i = 1 Hz − 10 Hz. The mean-mass air velocity is 8 ms^{-1}; the ratio of mean-mass velocities of liquid and gas phases is (0 ÷ 0.01). Depending on pulse duration the experimental data diverge significantly. The maximum of heat transfer coefficient is achieved for shorter pulses at relatively less rates of water mist impinging pulsed jet. Hence, the use of short pulses for liquid supply is the most efficient from the point of heat transfer enhancement.

The effect of the co-current air flow and pulsed mist jet on the heat transfer coefficient is presented in Figure 4. Dependence of the heat transfer coefficient on the single-phase air flow without droplets is displayed in the Figure (curve 1). The gas-droplets pulsed jets is shown in the Figure 4 by curves (2 - 5) for the conditions with frequency f_i = (1,2,3,5) Hz for the on-time of the pulse is t_{on} = 2 ms. A rise of the heat transfer coefficient at an increase in the air flow velocity is obvious for every pulse spray. The increase of frequency of pulses (f_i) and co-current air flow lead to enhancement of heat transfer rate. Thus, we can make the conclusion that the co-current air flow in the pulsed impinging spray increases heat transfer due to intensification of evaporation of liquid deposited onto the heat exchanger surface.

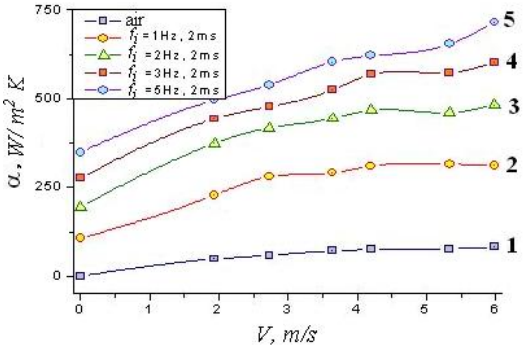

Figure 4 Dependence of heat transfer coefficient on air velocity.

Governing equations for the two-phase flow

In general, there are two approaches commonly used to predict particle motion in dilute fluid-particle flows. One method is known as Lagrangian or "tracking" scheme and another is named Eulerian or "two-fluid" model (see [16],[17]). Each scheme uses fundamentally different numerical methodology but the same underlying physical phenomena are addressed by both techniques. However, each method has advantages depending on the flow regime, computational resources, and information required.

In Eulerian formulation, the dispersed solid phase is treated as the second continuous fluid. The governing equations of particle motion have the similar differential form to fluid flow equations and separate boundary conditions are applied to each phase. The most noteworthy advantage of Eulerian scheme is that the solution to the equations of motion yields average flow conditions, such as particle concentration and velocity, in each computational cell. Eulerian model is computationally more efficient compared with its Lagrangian counterpart. The interaction between phases (coupling) is easily considered in Eulerian models by the addition of extra terms in the relevant equations. Moreover, the numerical procedures utilized to solve the fluid phase equations can also be applied to the solid phase.

Flow dynamics and heat transfer in the impinging pulsed gas-droplets jet were obtained with the use of the Eulerian approach initially developed by [18],[19],[20] for description of turbulent flows with solid particles

without heat transfer between the phases. The authors used the method for description of the gas-droplets impinging steady-state impinging gas-droplets jet [21]. The set of boundary conditions for dispersed phase in this Eulerian model had the form by [20].

The axisymmetric impinging intermittent jet is vertically injected from the pipe exit cross-section. The target is horizontal flat plate with constant wall temperature T_W = const. The air flow was assumed to be incompressible and Newtonian with temperature dependent fluid properties, and the viscous forces were negligible. Due to geometric and flow symmetry, only the flow field within the half domain is solved. To describe dynamics and heat and mass transfer in the axisymmetric non-steady-state gas-droplets flow, the system of Reynolds averaged Navier-Stokes (RANS) equations.

The main assumption of the work is the particles deposited on the wall from the two-phase flow momentarily evaporate, leaving the wall surface always dry. This assumption is quite valid for heated surface and used if the difference between wall temperature T_W and droplet temperature T_{WL} is $T_W - T_{WL} \geq 40$. The mass concentration of particles decreases in the downstream direction due to their deposition onto the plate surface and due to wall jet expansion. The droplet temperature is assumed to be uniform over the droplet radius and droplets are considered as spherical. The volume concentration of the dispersed phase $\Phi < 10^{-4}$ is assumed to be sufficiently small so inter-particle collisions can be neglected and the initial droplet diameter being $d_1 \leq 100$ μm. No coalescence occurs in the flow because the amount of the dispersed phase is small, and droplets never undergo brake-up. Weber number, based on the wall conditions $\mathrm{We}_W = \rho_W |U_L|^2 d_W / \sigma_W < 1$.

Second-Moment Closure Model for Two-Phase Flow

In second-moment turbulences, the Reynolds stress is obtained directly from solutions to modeled partial differential equations. In literature this approach is also called the Second Moment Closure (SMC), and the authors of this study will used this term. In order to deal the flow with anisotropic and nonequilibrium with multiscale integral and dissipation length scales, the SMC, is considered in this study. In the study we used the model developed by [22] which is developed for the impinging jet. The two-way coupling model of [19] is used along with the particulate feedback onto the mean distribution of the gas phase. The set of Reynolds stress equations $\langle u_i' u_j' \rangle$ and equation of the dissipation rate of the turbulent kinetic energy (TKE) of the gaseous phase were written

$$\frac{\mathrm{D}}{\mathrm{D}t}\langle u_i' u_j' \rangle = d_{ij} + P_{ij} + A_{ij} - \varepsilon_{ij} - A_{dp}\,.$$

$$\frac{\mathrm{D}\varepsilon}{\mathrm{D}t} = \frac{\varepsilon}{k}\left(C_{\varepsilon 1} P_k - C_{\varepsilon 2}\varepsilon\right) - \frac{\partial}{\partial x_k}\left[C_\varepsilon \langle u_l' u_k' \rangle \frac{k}{\varepsilon}\frac{\partial \varepsilon}{\partial x_l}\right] - \varepsilon_{dp}\,. \qquad (1)$$

Here $\frac{\mathrm{D}}{\mathrm{D}t} = \frac{\partial}{\partial t} + U_j \frac{\partial}{\partial x_j}$, d_{ij} is the diffusion term of Reynolds turbulent stress, P_{ij} is the stress production term, A_{ij} the wall-reflection contribution, ε_{ij} is the dissipation rate of Reynolds turbulent stress, A_{dp} and ε_{dp} is the effect of particles on carrier phase turbulence by [18] and $P_k = \nu_T \left(\frac{\partial U_i}{\partial x_j} + \frac{\partial U_j}{\partial x_i}\right)\frac{\partial U_i}{\partial x_j}$ is the turbulence generation rate.

Last terms in both equations of system (1) include an additional summand for description of interfacial coupling. The first equation of system (1) together with the standard terms describing turbulent diffusion, production of turbulent stresses from the shear averaged motion, redistribution of pulsation energy between different components of velocity fluctuations caused by correlation of pressure and deformation rate pulsations, and viscous dissipation, includes interfacial interaction A_{dp}.

The Influence of the Dispersed Phase on Gas Turbulence

The effect of the presence of dispersed phase on the gas phase Reynolds stress and rate of the dissipation has the form:

$$A_{dp} = \frac{2\rho_L \Phi}{\rho\tau}\left(1 - f_u\right)\langle u_i' u_j' \rangle - \frac{\rho_L}{\rho}\left(\Omega^{\varepsilon L}/\tau - f_u\left[\langle u_i' u_k' \rangle\, U_i - U_{iL}\right]\right)\frac{\partial \Phi}{\partial x_k},$$

$$\varepsilon_{dp} = \frac{2\rho_L \varepsilon}{\rho\tau}\left[\Phi\left(1 - f_\varepsilon\right) - \frac{\tau}{3}\left(\Omega^{\varepsilon}/\tau - f_\varepsilon\right)\left(U_k - U_{kL}\right)\frac{\partial \Phi}{\partial x_k}\right].$$

here $\Phi = M_L\rho/\rho_L$ is volumetric concentration of dispersed phase, $f_u = 1-\exp\ -\Omega^L/\tau$, $\tau = \dfrac{\rho_L d^2}{18\mu W}$ is the relaxation time of droplets, $W = 1+2\mathrm{Re}_L^{2/3}/3$, $\mathrm{Re}_L = \left|\vec{U}-\vec{U}_L\right| d/\nu$ is Reynolds number of dispersed phase, $\Omega^L = 0.608\Omega^E$, $\Omega^E = 0.22k/\varepsilon$ are Lagrangian and Eulerian time scales and $\Omega^\varepsilon = 15\nu/\varepsilon^{1/2}$ is time microscale of turbulence of [18], $\Omega^{\varepsilon L}$ is the time of droplet interaction with turbulent vortex [20]:

$$\Omega^{\varepsilon L} = \begin{cases} \Omega^E, & \left|\vec{U}-\vec{U}_L\right|\Omega^E \le \Gamma^E \\ \Gamma^E/\left|\vec{U}-\vec{U}_L\right|, & \left|\vec{U}-\vec{U}_L\right|\Omega^E > \Gamma^E \end{cases},$$

where $\Gamma^E = 2 < u^2 >^{1/2} \Omega^L$ is the turbulent length macroscale, Ω^L=0.608Ω^E and $\Omega^E = 0.22k/\varepsilon$ are Lagrangian and Eulerian time macroscales of turbulence. Here $f_\varepsilon = 1-\exp\ -\Omega_\varepsilon/\tau$, $g_\varepsilon = \Omega_\varepsilon/\tau - f_\varepsilon$ where $\Omega_\varepsilon = 15\nu/\varepsilon^{1/2}$ is the time microscale of turbulence [24].

Equations of the second moments of velocity pulsations $\langle u_{Li}u_{Lj}\rangle$, turbulent heat flux $\langle \theta_L u_{Lj}\rangle$ and droplet temperature fluctuations $\langle \theta_L^2\rangle$ have the form Zaichik [18].

Mean Equations for the Dispersed Phase

The system of mean equations describing momentum and energy transport in the dispersed phase haves the form [21]

$$\frac{\partial\ \rho_L U_{Lj}}{\partial x_j} = -\frac{6J\Phi}{d},$$

$$\frac{\partial\ \rho_L \Phi U_{Lj}U_{Li}}{\partial x_j} + \frac{\partial\ \rho_L \Phi < u_{Li}u_{Lj} >}{\partial x_j} = \Phi\ U_i - U_{Li}\ \frac{\rho_L}{\tau} + \Phi\rho_L g - \frac{1}{\tau}\frac{\partial\ \rho_L D_{Lij}\Phi}{\partial x_j},$$

$$\frac{\partial\ \rho_L \Phi U_{Lj}T_{Li}}{\partial x_j} + \frac{\partial}{\partial x_j}\ \rho_L \Phi < \theta u_{Lj} > = \Phi\ T_i - T_{Li}\ \frac{\rho_L}{\tau_\Theta} - \frac{1}{\tau_\Theta}\frac{\partial\ \rho_L D^\Theta_{Lij}\Phi}{\partial x_j},$$

where $D_{Lij} = \tau\ < u_{Li}u_{Lj} > + g_u < u_i u_j >$, $D^\Theta_{Lij} = \tau_\Theta < u_{Lj}t_L > + \tau g_{ut} < u_j t >$ are turbulent diffusivity tensor and particle turbulent heat transport tensor [19,20], $\tau_\Theta = \dfrac{C_{PL}\rho_L d^2}{12\lambda Y}$ is the thermal relaxation time, $Y = 1+0.3\mathrm{Re}_L^{1/2}\,\mathrm{Pr}^{1/3}$, and $g_{ut} = \Omega^{tL}/\tau_\Theta - 1 + \exp(-\Omega^{tL}/\tau_\Theta)$ is coefficient of particle involvement into pulsations of gas phase temperature. Ω^{tL} is time of interaction with temperature pulsations of the carrying flow. In the first approximation, let's take $\Omega^{tL} \approx \Omega^{\varepsilon L}$ according to [21]. Correlation functions f_u, f_ε, g_ε, f_{ut}, and g_u are the coefficients of droplet involvement into the macropulsation and micropulsation motion of the gas phase. In detail their assumptions used for their derivation are presented in [21].

Numerical Realization

Numerical solution is obtained by the method of finite volumes at staggered grid. For convective terms of differential equation s the QUICK procedure is used. For differential flows central differences are applied. The pressure field is corrected by the finite-volumetric agreed SIMPLEC procedure. Third-order upwind discretization scheme for the convective terms and second-order central difference for diffusion terms are used.

Computational domain is a cylinder with a size of 20*R* in a radial direction and height of *H*. The computational grid nonuniform both in axial and radial directions is applied. Fine grids are used near impinging surface,

jet axis and the pipe exit cross-section. At least 10 control volumes (CVs) have been generated to be able to resolve the mean velocity field and turbulent quantities in the viscosity-affected near-wall region ($y_+ < 10$). Grid sensitivity studies have been carried out to determine the optimum grid resolution that gives a mesh independent solution. All predictions are carried out on the grid with 200×256 CVs in axial and radial directions. Computations on the grid with 300×400 CVs are carried out additionally. The solutions presented here were considered grid independent.

The results of preliminary calculations for a single-phase flow in the pipe with the length of 150R are used for the gas phase velocity and turbulence on the pipe edge. This is enough to achieve a fully developed turbulent gas flow. The symmetry conditions are set on the jet axis for gas and dispersed phases. The no-slip conditions are set on the wall for the gas phase. Boundary conditions on the outer border of jet and impinging surface for dispersed phase correspond to the conditions of "absorbing surface" [21], when droplets do not return to the flow after the contact with wall or external border. On outer edge of the computational domain (the wall jet periphery) the conditions $\partial\phi/\partial r = 0$ for the all variables are set. The components of Reynolds stresses are determined at the same points on the control volume surface as the corresponding components of averaged gas velocities by the method of [22].

Results and Discussion

All computations are carried out for the single-phase air and gas-droplets mist impinging jets under the atmospheric pressure. The schematic of the impinging jet development is shown in the Figure 5.

The pipe diameter is $2R$ = 20 mm. The mean velocity of the gas flow on the axis of the pipe exit cross-section is U_{m1} = 17.5 ms^{-1}, Reynolds number for the gas phase is Re = $2RU_{m1}/\nu = 2.33\times10^4$. The dispersed phase is given as uniform distribution of parameters over the cross-section on the pipe edge. The initial velocity of dispersed phase is $U_{L1} = 0.8U_{m1}$. The initial size of droplets varies within d_1 = 0–100 μm, and its mass concentration varies within M_{L1} = 0–1 %. The wall temperature is T_W = 373 K, and initial gas and droplets temperatures are $T_1 = T_{L1}$ = 293 K. The distance between the pipe edge and target surface changes within $H/(2R) = 1 - 10$.

Frequency of pulsed flow was f_i = 0 – 60 Hz. The time of duty cycle of the flow DC was determined by the formula: $\mathrm{DC} = t_{on}/t_c = t_{on}/(t_{on}+t_{off})$, where t_{on} is time, when the flow is available (on-time), and t_{off} is the off-time, when there is no flow. In the study DC = 0.5 and we used in the computations only the rectangular form of the pulse (see Figure 6). The Strouhal number, determined by the tube diameter, is $\mathrm{St}_d = f_i 2R/U_{m1} = 5\times10^{-4} - 0.1$ and Strouhal number, calculated by the distance to the obstacle surface, is $\mathrm{St}_H = f_i H/U_{m1} = 6\times10^{-4} - 3.5$. This Strouhal number St_H shows how many times the gas flow reaches the plate surface during the cycle. All numerical simulations were performed for the rectangular shape of the intermittency both for the single-phase and mist impinging jets, and equal flow rates for the steady-state and pulsed impinging jets.

The Single-phase Air Impinging Pulsed Jet

The effect of impulse frequency on heat transfer in the stagnation point is given in the Figure 7. Experiments [6], [8] were performed for axisymmetric jet at Re = 7500, $\mathrm{St}_d = 2.4\times10^{-3}$–$7.6\times10^{-2}$, q_W = 420 W/m^2, $H/(2R)$ = 3 and $t_{on} = t_{off}$. Flow parameters in the pipe exit cross-section were set on the basis of preliminary calculation in the pipe with $2R$ = 15 mm diameter and 40R length. Here $\mathrm{ER} = Nu_{0,\,ns}/Nu_{0,\,st}$ is the heat transfer enhancement ratio. Here $\mathrm{Nu}_{0,\,ns}$ is Nusselt number in the intermittent impinging jet and $\mathrm{Nu}_{0,\,st}$ is heat transfer in the steady-state impinging jet. The time averaged Nusselt number was determined from relationship $\mathrm{Nu} = \frac{1}{TC}\int_0^{TC} \mathrm{Nu}(r,t)dt$ and TC is the period of time (minimum five time cycles).

Initially in the area of small frequencies (f_i < 5 Hz) heat transfer suppression is observed; at further increase of f_i the specific is heat transfer intensification (ER > 1.2 at f_i = 40 Hz). The results of our numerical calculations fairly correlate with the experiments [8] in the entire area of the studied frequencies f_i.

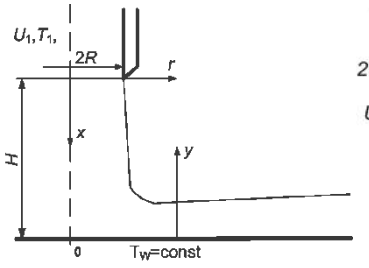

Figure 5 The schematic of the impinging jet development.

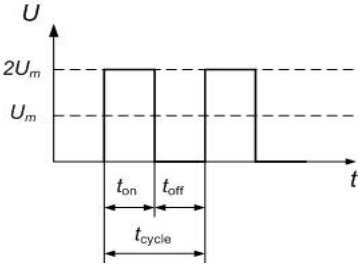

Figure 6 One period of the rectangular form of the pulse.

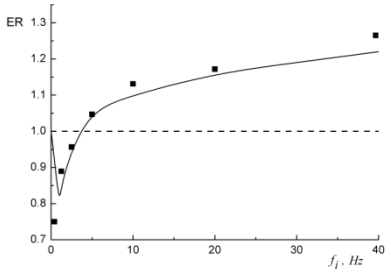

Figure 7 Distribution of heat transfer enhancement ratio in the stagnation point as a function of pulses frequencies. Points are the measurements by [6],[8], curve is the author's predictions.

Gas-Droplets Mist Pulsed Intermittent Impinging Jet

The second part of the paper is devoted to the numerical simulations of flow and heat transfer in the pulsed mist impinging jet.

Figures 8 show the effect of pulses frequency on the heat transfer rate along the target surface for $r/(2R)$ = 2 (a) и 6 (b). The time averaged local Nusselt number increases with frequency and Strouhal number. The heat transfer in the pulsed jet exceeds the corresponding value for the steady-state jet impingement in the case for relatively low spacing $r/(2R)$ = 2 (see Figure 8a) and it is lower than that one for the large distance $r/(2R)$ = 6 (see Figure 8b). The main regularities of the heat transfer behavior in the two-phase intermittent impinging jet are correlated with the regularities of heat transfer in the steady-state jet impingement [1], [2].

The comparison between our predictions and experiments for pulsed mist jet measurements was provided. These results are presented in the Figure 9. Here α is the heat transfer coefficient and J is the rate of the mist flow. Agreement between our computational results and our measurements was rather good especially for the small value of the time of the pulse t_{on} (line *1*) when the wall surface in the experiments is dry. The increase of t_{on} leads to the formation of liquid film and spots on target plate (observed in the measurements) and the residual between our simulations and experiments is rise (line *2*). We did not take into account the film formation on the wall from deposited droplets. We assumed droplets deposited onto the impinging surface momentarily evaporate (solid curves). The predictions without taking into account the heat spend the droplets heat up and evaporation q_{WL} (dashed curve) agreed better with measurements.

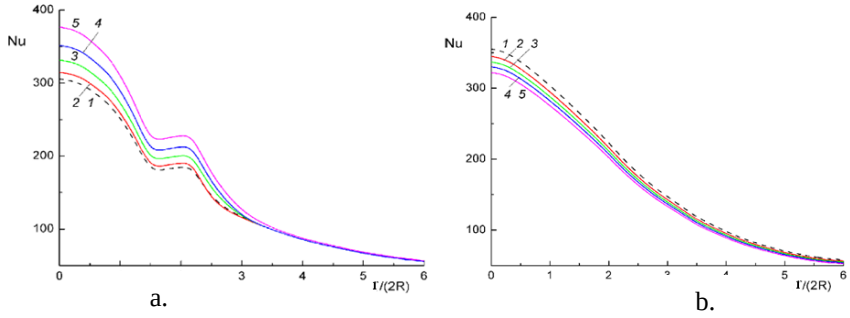

Figure 8 The effect of pulses frequency on the time averaged local heat transfer at $r/(2R)$ = 2 (a) и 6 (b). Re = 23000, d_1 = 50 μm, M_{L1}=0.01. *1* – f_i = 0 Hz (steady-state impinging jet); *2* – 5; *3* – 10; *4* – 30; *5* – 60.

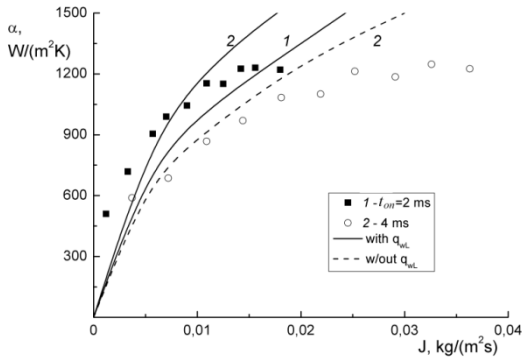

Figure 9 Heat transfer coefficient in pulsed mist impinging jet. Symbols are experimental results, curves are computations. H = 230 mm, f_i = 1 – 50 Hz, $T = T_\infty$ = 295 K, T_W = 373 K, U_{L1} = 14.8 m/s. *1* – t_{on} = 2 ms, *2* – 4.

Conclusions

The flow structure and heat transfer of an intermittent impinging mist jet is studied experimentally and numerically.

The experiment results we can conclude that the intensification of heat transfer by using of pulsed spray occurs when the surface of the heat exchanger has evaporation mode. The optimum ratio of flow rate of drip-

liquid phase of pulsed spray and velocity of cocurrent gas flow creates a condition of the evaporative regime on the surface of the heat exchanger.

Calculated results show in the range of distances between the tube edge and target $H/(2R) \leq 6$ heat transfer at stagnation point increases with a rise of pulsation frequency, whereas at high distances $H/(2R) > 8$ frequency rise causes heat transfer reduction. Heat transfer intensity during flow pulse action increases and exceeds significantly the corresponding value for the steady-state case. At time moment, when there is no flow, the value of Nusselt number decreases considerably. Results obtained are compared with available data of other authors, and satisfactory agreement is obtained for the influence of pulsation frequency on heat transfer of the gas jet with impinging surface.

Acknowledgements

This work was partially supported by the Russian Foundation for Basic Research (Project No. 12-08-00504).

References

[1] Martin, K., *Advances in Heat Transfer* 13: 1-60 (1977).
[2] Dyban, E.P., Mazur, A.I. *Convective Heat Transfer in Jet Flows around Bodies*, Kiev: Naukova Dumka, 1982. (in Russian).
[3] Jambunathan, K., Lai, E., Moss, M.A., Button, B.L., *International Journal of Heat and Fluid Flow* 13: 106-115 (1992).
[4] Zuckerman, N., Lior, N., *Advances in Heat Transfer* 39; 565-631 (2006).
[5] Azevedo, L.F.A., Webb, B.M., Queiroz, M. *International Journal of Experimental and Thermal Fluid Science* 8: 206-213. (1994).
[6] Herwig, H., Middelberg, G., *Acta Mechanica* 201: 171-184 (2008).
[7] Hofmann, H.M., Movileanu, D.L., Kind, M., Martin, H., *International Journal of Heat and Mass Transfer* 50: 3638-3648 (2007).
[8] Middelberg, G., Herwig, H. *Heat Mass Transfer* 45: 1519-1532 (2009).
[9] Xu, P., Yu, B., Qiu, S.X., Poh, H.J., Mujumdar, A.S. *International Journal of Thermal Science* 49: 1247-1252 (2010).
[10] Moreira, A.L.N., Panao, M.R.O., *International Journal of Heat and Mass Transfer* 49: 4132-4151 (2006).
[11] Pavlova, A.A., Amitay, M., *Trans. ASME Journal of Heat Transfer*, 128: 897-907 (2006).
[12] Panao, M.R.O., and Moreira, A.L.N. *International Journal of Heat and Fluid Flow* 30: 117-130 (2009).
[13] Nazarov, A.D., Serov, A.F., Terekhov, V.I. and Sharov, K.A. *Journal Engineering Physics and Thermophysics* 82: 1160–1166 (2009).
[14] Nazarov, A.D., Serov, A.F., Bodrov, M.V. *Technical Physics* 55: 724-727 (2010).
[15] Mityakov V.Yu., *PhD thesis*, St. Petersburg State Polytechnic University, (2005).
[16] Drew, D.A., *Annular Review of Fluid Mechanics* 15: 261-291 (1983).
[17] Crowe, C.T., Sommerfeld, M., Tsuji, T., *Fundamentals of Gas-Particle and Gas-Droplet Flows*, Boca Raton: CRC Press, FL, USA, 1998.
[18] Derevich, I.V., Zaichik, L.I., *Fluid Dynamics* 23: 722-729 (1988).
[19] Zaichik, L.I., *Physics of Fluids*, 11: 1521-1534 (1999).
[20] Derevich, I.V., *International Journal of Heat and Mass Transfer* 43; 3709–3723 (2000).
[21] Pakhomov, M.A., Terekhov, V.I., *International Journal of Heat and Mass Transfer* 53; 3156-3165 (2010).
[22] Craft, T.J., Launder, B.E., *AIAA Journal*, 30: 2970-2972 (1992).